Cofactor Complexes of DesD, a Model Enzyme in the Virulence-Related NIS Synthetase Family

Katherine M. Hoffmann[*§], Eliana S. Goncuian[§], Kimya L. Karimi[§], Caroline R. Amendola[≠], Yasi Mojab[§], Kaitlin M. Wood[≠], Gregory A. Prussia[≠], Jay Nix[α], Margaret Yamamoto[≠], Kiera Lathan[§], Iris W. Orion[≠]*

*author to whom correspondence should be addressed; email address: khoffmann@callutheran.edu; phone (805) 493-3916; fax (805) 493 -3392

[§]Department of Chemistry, California Lutheran University, 60 W. Olsen Rd. #3700, Thousand Oaks, California 91360, United States

[≠] Department of Chemistry and Biochemistry, 502 East Boone Avenue, Spokane, Washington 99258, United States

[α]Advanced Light Source 1 Cyclotron Road Lawrence Berkeley National Laboratory Berkeley, CA 94720, United States

Abstract: The understudied NIS Synthetase family have been increasingly associated with virulence in bacterial species, due to their key role in the synthesis of hydroxamate and carboxylate "stealth" siderophores. We have identified a model family member, DesD from *Streptomyces coelicolor,* to characterize structurally using a combination of wild-type and Arg306Gln variant in *apo*, cofactor product AMP-bound, and cofactor reactant ATP-bound complexes. Kinetics in the family have been limited by solubility and reporter assays, so we have developed a label-free kinetics assay utilizing a single-injection isothermal titration calorimetry-based method. We report second order rate constants 50-fold higher than the previous estimations for DesD. Our Arg306Gln DesD variant was also tested in identical buffer and substrate conditions, and confirmed undetectable activity. These are the first reported structures for DesD, and they describe the critical cofactor coordination. This is also the first label-free assay to unambiguously determine kinetics for an NIS synthetase.

Introduction:

Microbial iron compounds are essential to metabolic processes, but while iron in the environment itself is abundant (Fe^{3+} ion in particular), it is not readily available to most microorganisms due to limited solubility (10^{-18} M at neutral pH.)[1, 2] The bacterial strategy to compete for iron involves the synthesis and secretion of high-affinity small-molecule chelators called siderophores.[3] Siderophores are generally 500-1,000 Da in molecular mass, significantly increase Fe^{3+} ion's solubility, and may achieve association constants as high as 10^{24} M^{-1}.[1, 2]

Aerobic bacteria, facilitative anaerobic bacteria, fungi, and some plants commonly produce at least one siderophore.[1] Several hundred variations have been isolated[4], and sometimes several siderophores are discovered in the same organism--this apparent functional duplication allows for pathogenic bacteria to circumvent host defenses with varying structures.[5] Most siderophores are

constructed from common metabolic intermediates or derivatives, linked via peptide bonds to form small hexa-dentate chelators, but the functional group ligands vary.[6]

Several pathways exist for siderophore creation out of three different functional groups. The understudied Non-ribosomal peptide synthetase Independent Siderophore (NIS) synthesis products evade the human immune system[7], and are critical for survival[4, 8] and virulence[9-14] in iron limiting conditions. The pathways utilize hydroxamate or carboxylate functional groups, and are intriguing new anti-bacterial drug targets.[15]

While scientists have known about NIS products for over forty years, and even utilized the desferrioxamine B siderophore (dfoB,) and others for treatment of iron toxicity,[16-18] interest in the biosynthesis only recently increased as a result of observations that NIS siderophores are not recognized by the innate human immune system protein Siderocalin, conferring critical virulence to some of the most problematic pathogens.[7, 9, 19] NIS biosynthesis includes remarkable basic biochemistry in its own right, however. Peptide bonds are formed outside of ribosomes but without large protein complexes; instead, NIS siderophores are formed in small, soluble proteins with no useful homology to any other enzymes.[4, 14]

There is at least one member of a novel family of proteins (NIS synthetases) per each NIS synthesis pathway, playing a critical role of condensing a carboxylic acid with an amine (or, rarely, an alcohol) forming a peptide or ester bond.[4, 14] NIS synthetases are widely distributed: there are more than 80 proteins from at least 40 different bacteria which share up to 42% identity.[4] On the basis of high sequence identity and some known functions, several subtypes, A, A' B, C, were predicted to have different carboxylic acid specificities.[4, 14] Substrate specificities for one type A and several type Cs have been experimentally validated using mass spectrometry or qualitative binding assays; existing work suggests every NIS sythetase binds ATP as a cofactor, and produces AMP and PP_i.[20-26]

Interestingly, a sub-population of the NIS family are iterative enzymes, meaning they catalyze multiple condensation reactions on the same substrate, leading to a recent proposal to create a new subtype: C' for dimerization and macrocyclization of complex amine or amide intermediates[27]. These iterative enzymes

have broader substrate specificities than most, possibly a result of recognizing the progressively larger substrates,[21, 22] even though they catalyze precise enantioselective reactions.[21, 22, 25] There are iterative enzymes in several subtypes, however: the best characterized are in type A, for which AcsD (from *Pectobacterium chrysanthemi* and *Dickeya dadantii*) is the best model, and C', where DesD from *Streptomyces* species [4, 21] is the best characterized. The kinetics have been completed for AcsD with one of its substrates limiting (citrate, with a k_{cat} of 2.2 x 10^3 s^{-1}, and a K_m of 14.7 mM)[26], but not the other, and the kinetics have been attempted for DesD [21](inconclusive results), but no standard kinetic assay exists for the field, so each is completed with a different analog or reporter required.

Structures of four NIS synthetases have been solved and published, revealing a novel fold and novel ATP binding site, but none characterize fully the cofactor binding site flexibility, which should transition from *apo* to ATP-bound, to AMP-bound. One structure available is for the Type A AcsD involved in acromobactin synthesis in *Pectobacterium chrysanthemi* and *Dickeya dadantii* which was solved unbound to substrates (*apo*), bound to ATP, bound to adenosine and citrate,[26] and bound to a product analog: citryl-ethylenediamine.[25] Type C AsbB (from *Bacillus anthracis*), part of a mixed NRPS and NIS enzyme containing pathway, was crystallized with ADP, but in the same binding pocket defined by AcsD, and coordinated to homologous residues.[28] IucC[29] and IucA[30] were each crystallized with ATP only, despite attempts at co-crystallization. DfoC, a multi-enzyme NIS synthetase with an acyl-transferase domain and a NIS synthetase domain homologous to DesD, was crystallized in *apo* form[31]. These structures consistently reveal a novel NIS synthetase fold: three α/β domains in an overall shape approximating a cupped hand, with ATP binding at the bottom of a deep, bowl-like pocket of charged residues in the palm of the hand (figure 1).

Solution-based size exclusion experiments have confirmed that a dimer, or a mixture of monomers and dimers, is the relevant quaternary structure,[21, 25, 26, 28] for most, but not all[29-31] of the structurally characterized family members. This common dimer has an interesting feature: a solvent lined channel connecting active sites, but with no known function[28, 32]. Interestingly, IucA and IucC from *E.*

coli, were crystallized in tetramers; although SAXS data supported IucA's tetramer as the biologically relevant unit, IucC was determined to be a dimer that resembled the interface seen in AsbB and AlcC.[29, 30] AcsD crystallized in an unusual dimer with a relatively small (823 Å) dimerization interface. DfoC uniquely crystallized as a monomer.[31] Interestingly, in each of the published structures, despite the protein oligomer and ATP binding in all active sites, substrate or ligand was only found in one active site, if at all,.[25, 26, 28] This statistical disorder may explain why the structures of complexes have been elusive.

The mechanism has not been fully described, but it is proposed to include a covalently-bound adenylate intermediate[21], suggesting that understanding the binding and coordination of the cofactor will be critical to understanding or inhibiting the NIS Synthetase family. The adenylate intermediate may explain the unusual alpha-beta phosphate bond cleavage of the cofactor, and it also suggests a two-step mechanism[25]: the first establishing the adenylate intermediate with the carboxylate substrate, and the second exchanging the adenylate bond for a peptide bond with the amine substrate. While several conserved residues are observed in the active site, His443 and Arg306 (DesD numbering) alone have been established in AsbB and AcsD to have impaired the adenylation step of catalysis.[28] Additionally, in AcsD, Glu442 is hypothesized to be a catalytic general base for the second step, with activation from Arg501, both of which were catalytically incompetent or impaired when mutated conservatively in AcsD[25]. However, Arg 501 is not conserved in the family or in Type A, and Glu442 is incompletely conserved—the closest aligned (Figure S3) glutamate in DesD is Glu445, which is downstream from the well conserved His443 rather than the upstream neighbor, and well-conserved in the family as either Glu or Gln. No major conformational changes are observed in the cofactor or carboxylate bound proteins compared with *apo* structures (for AcsD, the RMSD of C_α is 0.4 Å for 573 atoms in *apo* vs. ATP-bound)[25].

There is no p-loop or Rossman fold in the cofactor recognition pocket, consistent with the completely novel fold. The conformation of ATP in the phosphate groups evidences compressed angles at the phosphorous atoms (~100° in IucA structure 5JM8) but strained and elongated ester angles, closer to 125°.[30] There is also a water network buried under the gamma phosphate in a basic-rich environment,

which was postulated to be where the pyrophosphate product would rest until released at the end of the turnover.[30] The carboxylate substrate (based on the AcsD structures) binds directly above the ATP, interacting with the postulated general base Glu442 and positioned well for the formation of the adenylate-citryl bond to form between the enantiospecific carboxyl oxygen and the alpha phosphate of ATP.[25, 26] These and other studies suggest that cofactor is bound first and released last from the binding site during catalytic turnover, arguably defining the electrostatic landscape of the binding site. Understanding the cofactor interaction with the pocket will be integral to a full understanding of NIS synthetase function.

Several kinetic assays have been developed including an NADH coupled fluorescence assay to measure product cofactor production in the presence of various nucleophiles, and a continuous coupled assay for PP_i production[33] to measure the rate of ATP turnover and establish that the cleaved phosphate bond produces AMP and PP_i, not ADP and P_i. Each of these are limited by the reporter in the assay. Additionally, a nucleophilic analog, hydroxamate, can be used to test cofactor or carboxylate preference, provided the enzyme can bind the analog as a tolerable substitute for its amine substrate[20]. With these assays, the field has determined catalytic rates ranging from 0.23 to 0.9 s^{-1} and Michaelis constants (K_M) of 0.2 – 6 mM.[21, 28, 30] An exception is AcsD, whose carboxylate substrate kinetics revealed a k_{cat} of 2.2 x 10^3 s^{-1} and K_M of 14.7 mM.[26] In that case, the second order rate constants were nearly 50x what had been reported for the family on average, but also evidenced was significant apparent product-inhibition creating non-Michaelis Menten kinetics curves. This difference highlights the need for a label-free assay and conditions that permit unambiguous determination of kinetic constants.

Desferrioxamines (dfo) are well-known members of the NIS siderophore subfamily consisting of alternating diamine and dicarboxylic acid building blocks linked by peptide bonds (scheme 1). Dfos are among the strongest hydroxamate siderophores known with formation constants of $10^{30.6}$-$10^{32.5}$.[34] DfoE (also called norcardamine) was first isolated from *Streptomyces* species,[35] but subsequently found in many other bacteria, including *Pantoea agglomerans*,[36] *Pseudomonas stutzeri*,[37] *Hafnia alvei*,[38] and *Erwinia*

amylovora[39]. *Streptomyces* species have been reported to produce a mixture of dfos in iron-limiting conditions, including dfoB, dfoG_1 and dfoE: dfoB is notable for its clinical importance as Desferal for the treatment of iron overload,[40] as an antimalarial[41, 42] and in anticancer[43] cocktail treatments.

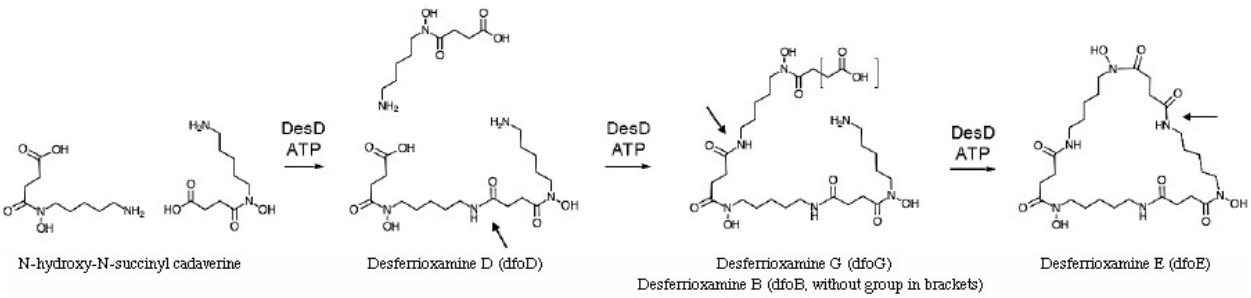

Scheme 1: Type C NIS synthetase DesD catalyzes three iterative or sequential peptide bonds (indicated with arrows) between three N-hydroxy-N-succinyl cadaverine (HSC) substrates. In step one, two HSC molecules are joined to form desferrioxamine D (dfoD), which in step 2 is connected to a third molecule of HSC to form desferrioxamine G (dfoG). The final step cyclizes dfoG to form desferrioxamine E (dfoE). Each bond formation event requires a stoichiometric equivalent of ATP to drive the reaction. Desferrioxiamines G and E as well as the version of dfoG lacking the reactive succinyl group, desferrioxamine B[18], are available commercially.

The study of dfos in treatment was not matched by the attention to their biosynthesis for many years, despite the growing interest in NIS synthetases as potential drug targets[15]. The central role of NIS synthetase DesD in dfo biosynthesis represents a model potential drug target; an opportunity to take advantage of unique chemistry and structural fold, and essential nature of NIS siderophores under iron-limiting conditions. [4, 8, 10-15]

Each of the multiple dfos observed in *Streptomyces* are all intermediates or products of the iterative turnover by DesD. More recent literature reveals that the synthesis of dfoE begins with lysine, which is decarboxylated (DesA), hydroxylated (DesB), and succinylated (DesC) to form N-hydroxy, N-succinylcadaverine (HSC) in the first three steps of the pathway.[5, 39] DesD, the only NIS synthetase in the

operon, is the enzymatic catalyst for the final three steps (scheme 1) in the creation of cyclic dfoE, and so must sequentially bind the small HSC, the dimerized intermediate (dfoD), and the linear trimer (dfoG) in order to complete the cyclic dfoE. Previous biochemical characterization of DesD has established the substrates, products, and analogs that may be bound in high concentrations, and that that the selectivity of the binding site is broad under these conditions[21, 44]. Additionally, the iterative intermediates of dfoE production, the dimer and trimer linear intermediates, are released between bond formation event[21, 44]. Estimates of kinetic constants were made using an analog-based assay, but apparent non-Michaelis-Menten cooperativity, and (like AcsD) apparent substrate inhibition made kinetic analysis challenging[21, 44].

We present the first structures of DesD in *apo*, co-factor and co-factor product bound complexes. We have structurally characterized an Arg306 variant, utilized to impede kinetic turnover for these structural studies, and additionally present the ITC-based kinetics of both *wt*, and Arg306Gln DesD. This kinetic assay is the first label-free assay for the NIS field, which may allow for more detailed kinetic comparisons in the future, and may have broader use for iterative enzymes in general.

Materials/Experimental Details:

Expression and Purification of Recombinant Enzymes. Site-directed mutations were constructed using megaprimer PCR [45] with *Pfx* DNA polymerase (Stratagene) polymerase and commercial oligonucleotides (Integrated DNA Techonolgies). For mutation Arg306Gln, a mutant oligonucleotide[3] 5'-TGGGCTTTATGCAGGGGCTTTCA-3' was paired with the 3' oligonucleotide primer DESDEND (5'-CTACTCGAGCCTCGACCTG-3) over the *E.coli* expression optimized C-terminal His-tagged DesD plasmid (Blue Heron Synthesis) in the first PCR reaction to give a 200 bp product. This PCR product was used as a megaprimer in a second PCR reaction with the 5' oligonucleotide primer DESDSTART (5'-ATGTCGTTGGCGGATGCGGT-3') to create the final mutated DesD gene. The final PCR product was used as a megaprimer in a MEGAWHOP [46] PCR protocol. The expression plasmid was subjected to DNA

sequencing (Sanger Sequencing at Clemson University Genomics Institute) of the entire DesD gene to verify introduction of the correct mutation.

Expression, purification, storage and quantification of Arg306Gln and wild-type DesD (UniProt accession no Q9L069_STRCO) were identical. Single colonies of freshly transformed plasmids in XJb cells (Zymo Research) of LB media with 50 μg/mL ampicillin plates were selected to grow in 10 mL overnight LB media with 50 μg/mL ampicillin cultures. These were used to inoculate 1 L of terrific broth containing 50 mg/L Amp and 3 mM arabinose, grown to OD_{600}= 0.6-0.8 at 37°C with shaking. At this point, the cultures were cooled to 15°C, and overexpression was induced with 0.5 mM IPTG overnight. Cells were pelleted, quantified, and stored at -80°C. To purify, crude homogenates of overexpressed protein were created by resuspending in buffer A (0.020 M Tris-HCl pH 8.0, 200 mM NaCl, 10% glycerol, 5 mM Imidazole) containing 1 mg/L DNAse I and protease inhibitors (VWR), and purified to homogeneity by affinity column chromatography (GE HisTrap HP 5 mL) using a gradient of imidazole from 0.040M – 0.500M in buffer A, followed by a desalting column (HiPrep 26/10 Desalting) using an AKTA Start FPLC (GE Healthcare). All proteins were quantified by UV absorbance at 280 nM based on the calculated molar absorptivity of 90,760 $M^{-1}cm^{-1}$, and purity was confirmed by SDS-PAGE and a molar mass of 67,556.4 g/mol. Protein was stored in 25% glycerol containing buffer A at 4°C for up to one weeks. Typical yields were 5 mg of pure protein from a liter of cells.

Crystallographic Methods. Single, three-dimensional crystals of wt DesD cocrystallized with DesC and 0.5 M ATP/0.5 M cadaverine/0.5 M succinyl CoA, were grown over several days in .16 M $MgCl_2$, 20% PEG 4000, 20% glycerol, 10% ethylene glycol and 0.08 M TRIS hexahydrate pH 8.5 with 10 mg/mL each protein at 22°C using hanging drop vapor diffusion. Crystals were soaked in artificial mother liquor containing 40% glycerol for 30 seconds prior to flash cooling in liquid nitrogen. *Apo* crystals of R306Q DesD, and R306Q cocrystallized with ATP were grown in the same well solution lacking ethylene glycol, and including 24% (apo) or 25% (co-crystal) PEG 4,000. R306Q co-crystallized with ATP was additionally soaked with 1 mM dfoB substrate for 1 minute prior to flash cooling in liquid nitrogen.

Data collection for wt DesD-AMP structure was carried out on an R-Axis HTC system using a FRE dual source for Cu-Kα (1.54 Å). Data collection for all other crystals were collected at the Advanced Light Source Beamline 4.2.2 and reduced and scaled using HKL2000[47]. Data were processed using Mosflm[48], and an initial molecular replacement solution was obtained by using a search model derived from a single dimer of AsbB (PDB 3TO3) in Phaser [49]. The initial solution was subjected to multiple rounds of refinement using Refmac5 [50] and model-building in Coot [51, 52]. Final refinement incorporated TLS [53] with one TLS group per protein chain. Simulated annealing omit maps ($2F_o$-F_c difference Fourier maps) and PDB_redo[54] were used to verify the correctness of the models and presence of ligands; superposition of cofactor-bound and *apo* DesD was done using the program Gesamt[55] in the CCP4 suite of programs. Crystallographic coordinates and structure factors for wild type DesD/AMP (Protein Data Bank code 6P63), *apo* Arg306Gln DesD (Protein Data Bank code 6NL2), and Arg306Gln DesD/ATP (Protein Data Bank code 6XRC) have been deposited in the Protein Data Bank (rcsb.org)[56]. Refinement statistics are listed in Table 1.

Enzyme Kinetics. All ITC experiments were performed in 50 mM HEPES buffer at pH 7.5, containing 150 mM NaCl, 5 mM TCEP, 15 mM $MgCl_2$ and 25% glycerol, with care taken to avoid metal contamination from glassware. In order to derive the kinetic parameters of the DesD catalyzed macrocyclization (the last step of scheme 1), ITC data were obtained from a single injection of concentrated DesD enzyme for a final concentration of 1 μM. The binding cell contained 1 mM dfoG and 5 mM ATP, or 1 mM dfoG and 0.5 mM ATP, and was monitored continuously for differences in thermal power (dQ/dt) as the substrate was fully depleted, which is proportional to rate according to equation 1, below:

$$Rate(\vartheta) = \frac{\frac{1}{V * \Delta H_{app}} * dQ}{dt} \quad (1)$$

where V is the cell volume (~280 μL) and ΔH_{app} is the total molar enthalpy for the solution. The raw data thermogram reflects a reaction where the substrate is completely consumed, allowing the calculation of total Q, and consequently, the total enthalpy change in the calorimeter (ΔH_{app}.) Since the ΔH_{app} reflects the sum of the enthalpy of the reaction (ΔH_{rxn}) as well as the enthalpy of ionization from acid base groups (ΔH_{Ion}), ΔH_{Ion} was determined for our heat-deactivated enzyme in our buffer system in a separate control run, and was the primary method for determining the cell vs. syringe chemical organization (there was significant ΔH_{Ion} in the dfoG and ATP dilution, and insignificant ΔH_{Ion} of enzyme dilution). Analysis [34] was performed using Graphpad Prism 8.2, where $V_{max} = k_{cat}*[E]$ and the data were well-fit with nonlinear regression, below, to calculate k_{cat} and K_m values.

$$\vartheta = \frac{V_{max} * [S]^{\square}}{K_M^{\square} * [S]^{\square}} \quad (2)$$

Results:

Overexpression of C-terminal His-tagged wild-type DesD and variant Arg306Gln DesD

DesD overexpresses well and purifies between 3 and 10 mg of pure protein per liter of cell culture when tagged at the C-terminus, which unlike the N-terminal tag, does not interfere with the dimerization interface or solubility. DesD and variants are purified in a buffer containing 10% glycerol to optimize the function of the FPLC and chromatography, but must be immediately exchanged into 25% glycerol to stably maintain solubility for overnight storage at 4°C, crystallography, or ITC experiments at 37°C for more than 30 minutes. Stored this way, DesD is active for at least 9 days (based on kinetic data not shown.) DesD eluted from a calibrated gel exclusion column (Superdex 200, GE) at 140 kDa +/- 20 kDa, consistent with the size of a dimer, as well as a shoulder consistent with the size of the monomer on SDS PAGE denaturing gels (67 kDa, Figure S1).

To create a variant that could bind and trap substrate-bound complexes without kinetic turnover, we examined the alignment of DesD with AsbB[4], an NIS synthetase with published kinetic mutations and

structure (Figure S3). Arginine 306 was identified by alignment as the catalytic arginine, and mutated using site directed mutagenesis to the size-conserved variant of glutamine. Arg306Gln DesD overexpressed and purified as wild-type did, with structures confirming the location of 306 in the active site.

Table 1. Data collection and refinement statistics for DesD & variants[a]

	wt DesD + 500 mM AMP (PDB 6P63)	*Apo* R306Q DesD (PDB 6NL2)	R306Q DesD + 500 mM ATP (PDB 6XRC)
Wavelength (Å)	1.54	1.54	1.54
Space Group	$P12_11$	$P2_12_12$	$P2_12_12$
Cell parameters			
Cell edges (Å)	98.43, 74.24, 183.17	95.69, 181.62, 73.32	98.93, 183.37, 74.40
Angles (°)	90, 94.7, 90	90, 90, 90	90, 90, 90
Resolution (Å)	89.53-2.40	60.54-1.92	61.12-2.45
	(2.44-2.40)	(1.95-1.92)	(2.45-2.54)
Unique reflections	99,262	98,322	49,960
Redundancy	3.8 (3.9)	7.5 (7.5)	7.4 (7.5)
Completeness	96.2 (94.3)	100.0 (100.0)	99.9 (99.8)
R_{sym} or R_{merge} (%)	0.090 (0.344)	0.085 (0.219)	0.196 (0.439)
$\langle I \rangle / \langle \sigma I \rangle$[b]	9.5 (3.5)	15.8 (7.0)	5.0 (2.6)
Half-set correlation CC(1/2)	0.993 (0.841)	0.996 (0.945)	0.981 (0.949)
Reflections in test set	4971	4796	2494
R_{work} (%)	17.7	15.5	20.4
R_{free} (%)	21.5	18.3	27.3

No. of atoms			
Protein	36,477	18,241	18,239
Cofactor + ions	128	3	80
Glycerol	48	120	36
Solvent	738	737	729
B-factors			
Protein	24.14	20.47	24.26
Cofactor	24.04	N/A	59.76
Ions	30.44	21.07	50.28
Glycerol	29.32	28.31	44.89
Solvent	23.58	26.41	33.63
RSCC			
Cofactor	0.94		0.85
rmsd from ideal[c]			
Bond distance (Å)	0.0133	0.0157	0.0114
Bond angle (°)	1.833	1.871	1.714
Ramachandran plot outliers (%)[d]	0.80	0.68	0.42

[a] Values in parentheses represent data for the highest resolution shell.

[b] Reported as ‹‹I›/σ‹I›› in SCALA or SCALEPACK.

[c] Ideal values from Engh and Huber [57].

[d] Calculated using a strict boundary Ramachandran plot [52].

Crystal structures of wtDesD bound to AMP, apo Arg306Gln DesD, and Arg306Gln DesD complexed with ATP

To gain greater insight into the structural basis for the iterative behavior of DesD, the crystal structures of *apo*, a product cofactor (AMP) complex, and a reactant cofactor (ATP) complex were solved to between 1.7 and 2.5 Å resolution (Table 1). AMP is bound in the *wt* protein, the other two structures are solved with the DesD variant Arg306Gln. Each monomer of DesD, whether wildtype or variant, is similar in core fold to the solved structures of dfoC NIS domain from *Erwinia amylovora* (PDB 5O7O)[31], alcagin biosynthesis protein C (AlcC, unpublished, PDBs 2X0O, 2X0P, 2X0Q) from *Bordatella brochiseptica*, AcsD (2X3K, 2X3J, 2W02, 2W03, 2W04, 3FFE)[25, 26] from *Pectobaterium crysanthemi*, AsbB (3TO3)[28] from *Bacillus anthraxis* and IucC and A (6CN7, 5JM7, 5JM8)[29, 30] from *Klebsiella pneumoniae*. Of these, AsbB, AlcC, and IucC were also identified as a Type C NIS synthetases[4], like DesD. A monomer of the *apo* DesD protein superposes with ATP-bound IucC (6CN7) closely (rmsd 1.611 Å, over 594 C_α atoms) despite only a 31.5% identity in the primary structure.

Two chains of the DesD polypeptide occupy the asymmetric unit of the $P2_12_12$ spacegroup, which describes both the apo Arg306Gln DesD, and Arg306Gln DesD complexed with ATP structures. In the *wt* DesD bound to AMP structure, which crystallized in $P2_12_12_1$, four chains of polypeptide are present in the ASU. In both the Arg306Gln with ATP and the wt DesD with AMP structures, a substrate analog was soaked or co-crystalized with the protein, but were unable to be modeled with confidence. The DesD was always found as a dimer (figure 1), consistent with gel exclusion chromatography (Figure S1), although in the *apo* R306Q variant, the dimer is generated through symmetry operations. The DesD interface buries 2080 $Å^2$, consistent with the AlcC, IucC and AsbB structures. The generally observed solvent lined channel between active sites is not apparent in DesD—in both AMP and ATP bound structures, it is filled by a C-terminal loop comprising residues 569-582.

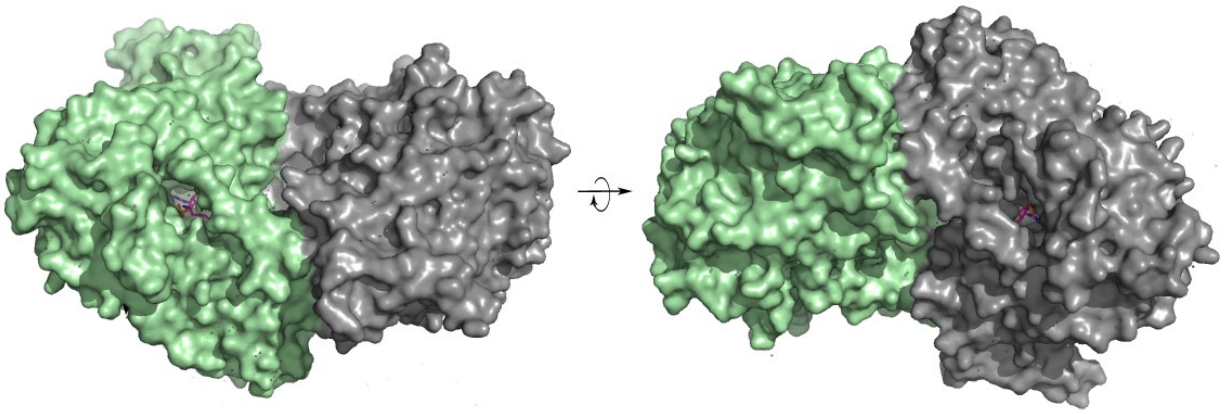

Figure 1: X-ray crystal structure of the DesD homodimer with AMP bound (magenta atom coloring). The two chains are colored green and grey, and rotated ~90° along the x-axis to show the active site entrance for each monomer. A C-terminal loop fills part of what has been observed as a solvent lined channel connecting the two active sites in other NIS Synthetases.

In the active site (figure 2) ATP or AMP are found in the same position and orientation in both complexes, surrounded by a number of direct or solvent-bridged contacts including Gln277, Arg306, Glu445, His443, Asn446 and Asp463. The strained angles on the ATP phosphates and bridge to Mg^{2+} from the alpha and gamma phosphates are consistent with NIS synthetase structures as well.[26, 30] The distances measured between the beta carbons of Arg306, His443, and Asp463 reveal minimal differences in binding site with substrate or cofactor association (figure 2c): Gln306 to His443 is 15.7 Å in the ATP complex (vs. 16.0 in *apo*,) His443 to Asp463 is 9.4 Å in both structures, and Asp463 to Gln306 is 12.3 Å (vs. 12.4 in *apo*). The occupancy of the cofactor in the binding site was confirmed with omit maps (Figure 2a-b and Figure S2.) Cofactors were modeled in every chain in both the wt DesD/AMP structure and in the R306Q DesD/ATP structure.

Interestingly, while AMP and ATP overlay well in the complex structures, the *apo* structure had a glycerol molecule and either one or two chloride ions in similar positions. Glycerol molecules were also found behind the adenine rings (both complexes) and below the phosphate groups in the ATP-bound

complex. Two molecules of symmetry related glycerol are also found in the dimerization interface in all structures. Notably, a high amount of glycerol is required for DesD solubility and is present in purification buffers as well as assay buffers and crystallization solutions.

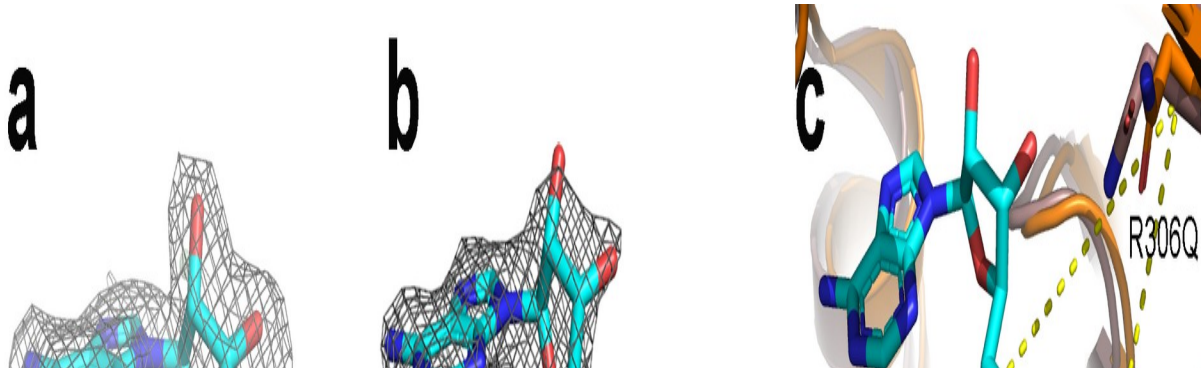

Figure 2. OMIT maps of DesD cofactors (turquoise atom coloring) and their location in the binding site. a) PDB 6P63 is bound to product cofactor AMP, shown in a $2F_o$-F_c OMIT map contoured at 1.0σ. Mg^{2+} is shown as a grey sphere. b) PDB 6XRC is bound to substrate cofactor ATP, also in a $2F_o$-F_c OMIT map contoured at 1.0σ. c) The distances measured between the beta carbons in the shown amino acids reveal that *apo* R306Q DesD (orange) has a nearly identical binding site to the R306Q DesD bound to ATP (purple). Distances between the beta carbons in Arg306Gln to His443 is 15.7 Å in the ATP complex (vs. 16.0 in apo,) His443 to Asp463 is 9.4 Å in both structures, and Asp463 to Gln306 is 12.3 Å (vs. 12.4 in apo).

Kinetic Studies of DesD catalyzing macrocyclization.

To overcome the limitations of DesD kinetic studies previously published, we developed a label-free calorimetry-based kinetics assay using isothermal titration calorimetry (ITC). The enzyme in the syringe in a concentrated stock was injected into cell containing substrate and cofactor pre-diluted. The background enthalpy of ionization in this orientation was able to be subtracted from the data (figure 3a). This organization was best suited to single injection kinetics, rather than multi-injection titrations, in which the rate is continuously calculated for depleting substrate concentration. Concentrations higher than 1 mM dfoG resulted in systematic oscillations in heat during equilibration, pre-experiment, that we

interpreted as dfoG and metal cell association and dissociation, a phenomenon that dissipated after 15 minutes but may be overcome in the future with pre-incubation of substrates.

The velocity vs. dfoG concentration graphs (Figure 3b) are well fit by a non-linear Michaelis-Menten curve. The data reveal a k_{cat} of 11.1 +/- 0.2 s^{-1}, and a K_m of 0.35 +/- 0.01 mM. The specificity constant, k_{cat}/K_m was 32,000 +/- 1,000, and the ΔH of turnover was -0.9 +/- 0.1 kJ. The velocity vs. ATP concentration graphs (Figure 3b) were also fit by a non-linear Michaelis-Menten curve, revealing a k_{cat} of 7.48 +/- 0.06 s^{-1}, and a K_m of 0.232 +/- 0.004 mM. The specificity constant, k_{cat}/K_m was 32,200 +/- 600 and the ΔH of turnover was 14 +/- 5 kJ. Arg306Gln DesD was tested in identical buffer and substrate conditions, and revealed negligible activity. Likewise heat-inactivated enzyme or titration into solvent (no substrates) resulted in baseline curves. These data are summarized in Table 2.

A

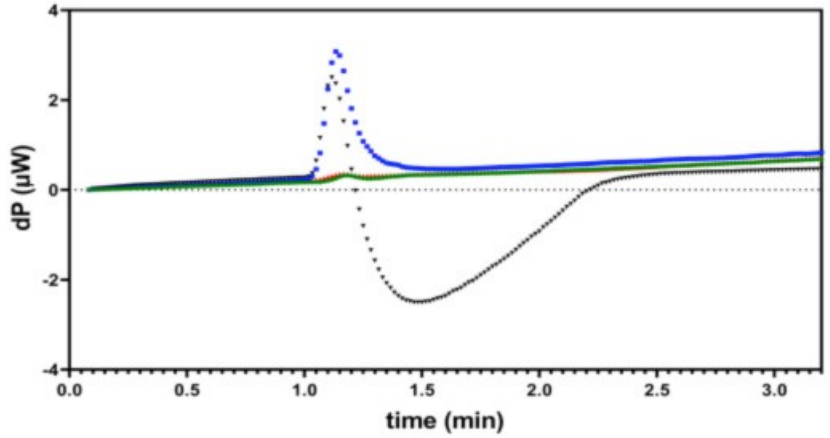

B

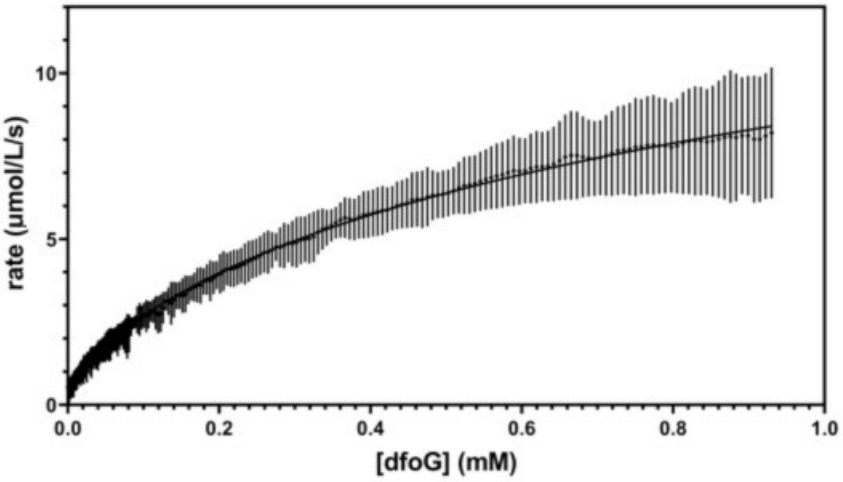

C

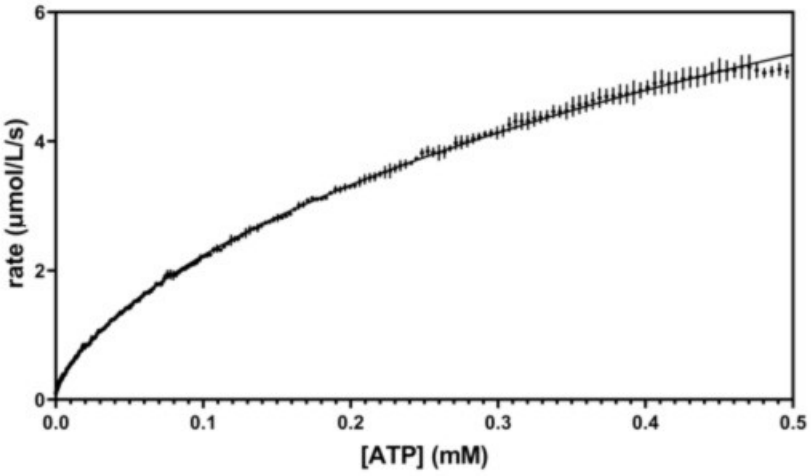

Figure 3: The data and v vs. [S] analysis for the continuous kinetic assay of wt DesD catalytic turnover of dfoG to dfoE. A) The exothermic reaction (negative dP required to maintain isothermal conditions) resulting from a single injection of wild type (black triangles) into a cell containing 1 mM dfoG and 5 mM ATP, was not observed in the Arg306Gln (red triangles), or heat-inactivated (green circles) DesD (1 μM) nor the the control run to estimate ΔH of enzyme dilution (blue squares). B) rate vs. [dfoG] with standard deviation error shown for four replicate runs. C) rate vs. [ATP] with standard deviation error shown for three replicate runs. The kinetics data were analyzed in GraphPad Prism 8.2.

Table 2: Reported Kinetic Constants for DesD

	k_{cat} (sec^{-1})	K_m (mM)	K_{cat}/K_M ($M^{-1}s^{-1}$)	ΔH (kJ/mol)
DesD (dfoG)	11.1 +/- 0.2	0.35 +/- 0.01	32,000 +/- 1,000	-0.91 +/- 0.1
DesD (ATP)	7.48 +/- 0.6	0.232 +/- 0.003	32,200 +/- 600	14 +/- 5

Discussion:

Construct and Purification

DesD overexpresses very well and purifies to 95% purity with a single metal affinity column, provided it is tagged on the C-terminus. In our initial work with DesD, we had tagged the N-terminus and discovered problems with inclusion bodies, purification, and solubility; these solubility issues were not resolved even when we attempted to cleave the tag.

DesD, AsbB and AlcC all crystallize as dimers with identical and compelling dimerization interfaces. All were confirmed by solution studies, and were all tagged at the C-terminus. AsbB made notable mention of the N-terminal construct being problematic for solubility or expression, which was similar to our experience. We note that the dimerization interface variation observed in the NIS synthetase family

correlates with N-terminal histidine tagging (the N-terminus is in the dimerization interface) and the absence of what is, in DesD, helix 1. Each of the unusual dimers or tetramers in the family: IucA, C and AcsD each lack the first 10 or so amino acids that in DesD and AsbB form the first short helix and contribute significantly to the AsbB and DesD described dimerization interface. We are confident, however, that the homodimer observed in our studies and consistent with the majority of the field is the biologically relevant oligomer for DesD.

Once we switched the construct to a C-terminal tag, we were able to over-express and purify DesD readily, but continued to observe a problem with solubility (visible white precipitate and lower concentration) in anything less than 25% glycerol for 30 minutes in kinetic assay conditions or crystallography conditions. We were able to maintain solubility in 25-30% glycerol conditions, and we suggest that solubility may explain the failed kinetics analysis in earlier literature for AcsD and DesD, which was interpreted at the time as product inhibition.

Binding sites

In both our ATP and AMP bound structures, the position of the adenosine, alpha phosphate and magnesium ion is consistent and overlays well (Figure 4a). There is a glycerol behind the adenine ring and under the phosphate (Figure 4a and c). The latter is very interesting as previous work has shown PP_i biproduct is bound and released with the final product at the end of turnover, and this glycerol is so well coordinated in the positively charged pocket it strongly supports the hypothesis that this is the PP_i location after the initial adenylate formation step in the mechanism.

ATP binding redefines the binding site electrostatics, covers the positively charged PP_i pocket with negatively charged phosphates, and establishes a potential network of hydrogen bonding and electrostatic contacts. ATP and AMP both appear at full occupancy in both sites of the DesD homodimer, suggesting that in the binding order, ATP binds first, and is covered with the substrate association filling the rest of the pocket. This order explains how the product cofactors of AMP and PP_i would stay bound until the release of all products at once at the end of turnover, but should be explored further in binding assays.

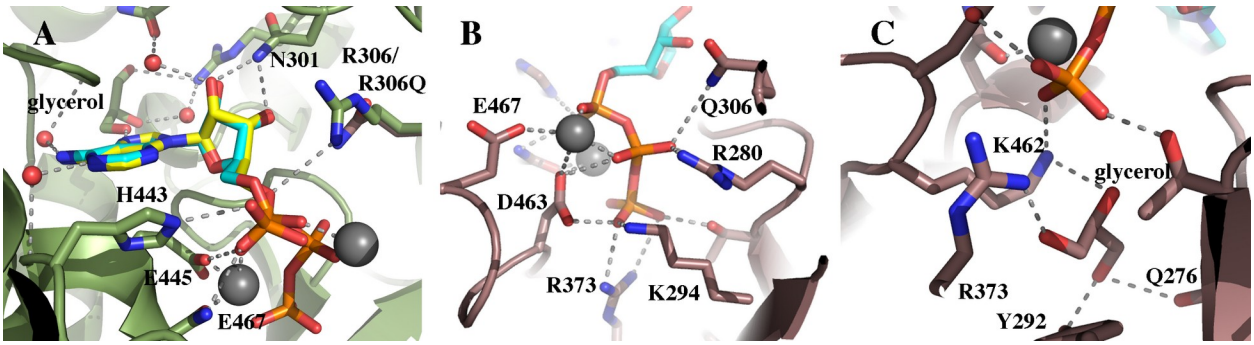

Figure 4. A comparison of electrostatic contacts in the cofactor-binding site. A) An overlay of AMP (yellow atom coloring) and ATP (turquoise atom coloring) in the wild-type binding site (green atom coloring), with the ubiquitous glycerol shown in green atom coloring behind the adenine ring, and the variant Arg306Gln shown in purple atom coloring. Electrostatic contacts across the AMP are conserved in both binding sites, and relevant side chains are shown in sticks (atom coloring). B) The phosphate contacts in the R306Q structure. Angles on the phosphates are under strain: with the esters stretched from 120 ° up to 130 ° /145° and the phosphates compressed to 100°. The pocket is polar or acidic near the magnesium ions, but transitions to basic towards the bottom of the pocket. C) The glycerol in the bottom of the phosphate binding pocket is well coordinated and may be displaced by PP_i over the course of the reaction.

The DesD phosphate binding contacts to ATP are consistent with the AMP contacts through the alpha phosphate, then add a magnesium ion and 9 new contacts, coordinating the last two phosphate groups well (Figure 4b). Analysis of the phosphate structure reveals a strain on the angles. Where IucC's ATP evidenced slightly stretched ester angles (125°), our structure saw them stretched to 130° for O_3P_β and 145° for O_3P_γ. This strain positions the alpha-beta bond near catalytic residues for the adenylate-formation step of the mechanism, but also suggests that the release of strain in the reactant-bound form may favor formation of the intermediate adenylate and product PP_i. This suggests intriguing possibility for mechanism since the formation of the adenylate intermediate might reposition the substrate by several Å

as it releases the strained alpha-beta phosphate bond, possibly rearranging the active site for the second step of the catalytic reaction with the amine functional group. Further research and structures would be needed to explore this possibility.

Based on the primary structure, we had successfully predicted that Arg306 would be in the position of the conserved arginine residues in NIS Synthetases. The variant of Arg403Gln did little to change the contacts in the cofactor binding site except to break one electrostatic contact to the alpha phosphate (Figure 4a)—likely critical for catalyzing the adenylate formation in what has been proposed to be an SN_2 type reaction[25].

An unpredicted critical active site residue was Glu467 (Figure 4a-b). Glu467 is in the functional role of residue Glu442 in AcsD, where the side chain in AcsD makes bidentate contacts to the product, but in our structure makes contacts to low B-factor water molecules (Figure 5). Further research will be needed to determine the role of Glu 467 in the mechanism, but based on the structure, we hypothesize that it is the proposed catalytic glutamate, which may also play a role in coordinating the amine substrate.

We had predicted, with no great confidence, that Glu445 would be in the physical position of the catalytic glutamate based on alignments, but have revealed that Glu445 is instead playing a critical role in magnesium and phosphate coordination (Figure 4a)—likely explaining the conservation. Additionally, Glu445 rotates 92 degrees (measured between C_{δ}-C_{γ}-$C_{\delta,}$, figure 5) on cofactor binding, rotating from a flexible orientation into the empty active site to a highly-coordinated position between the Mg^{2+} ion, the gamma phosphate, and His443. A comparison of *apo* to either of the bound structures also reveals a subtle loop to a single turn helix transition in the residue range of His443-Asn446 (figure 2c). We hypothesize that the Glu445 role in coordinating ATP directly triggers this increase in secondary structure, and may subtly position His443 for the second step of catalysis, but a co-complex structure of the substrates, transition states, or product states would be required to test the hypothesis.

Kinetics

KinITC represents a far superior technique for DesD kinetic characterization than the previous assays developed for the field. The hydroxamate assay developed for the family[20], and utilized well in IucA characterization, will not work for enzymes whose amines are too complex to be substituted by hydroxamate, or are attached to the carboxy substrate and therefore cannot be added separately. KinITC is in general a good option for kinetics analysis as no label is required (which removes the reporter limit for the detectable k_{cat}). It could therefore also replace (or complement) the continuous coupled assay utilized as an alternative to the hydroxamate assay.[29, 30, 32] To pilot this assay, we required 25% glycerol to stabilize our protein in buffer, hit a 1 mM limit to our dfoG substrate concentration before significant background interactions interfered, and discovered that significant background heat of dilution was generated when substrates (with many acid/base groups) were titrated into enzyme. Since we were unable to titrate substrates into dilute enzyme, we monitored kinetics after a single injection of enzyme into substrates (which had little background heat of dilution in controls.) Continuous monitoring of the power required to maintain the temperature during our enzyme reaction resulted in clear saturation curves for given concentrations of substrate (figure 3).

The velocity curves can be well fit with a classic Michaelis-Menten curve, and it will adequately fit the high substrate concentration points (within the standard deviation of the replicates), and through the K_M. However, in the equilibration of substrates with the cell, we observed a regular oscillation of signal that resolved in 10-15 minutes, but may be an artifact of dfoG interacting with the metal cell of the ITC instrument (a chelation equilibrium with iron that is competitive with the magnesium in the buffer). We suspected initially that our dfoG-Mg^{2+} interaction was influencing the available dfoG substrate population at low concentrations, but were unable to detect heat of binding using ITC in similar conditions. Possibly this variation could be resolved by pre-incubation with dfoG containing wash buffer prior to the experiment.

The v vs. [dfoG] curve, when fit with a classic Michaelis-Menten line of best fit, has a kinetic turnover of 11.1 +/- 0.2 sec^{-1}, which is much faster than the previously estimated k_{cat} of ~0.2 s^{-1}, and is substantially higher than the rest of the field with the exception of AcsD (2,200 s^{-1})[26]. AcsD kinetics were determined via label-free mass spectrometry analysis[26], and it, like DesD, is significantly faster than any of the studies conducted via the continuous coupled AMP production (NADH reporter) or hydroxamate assays. DesD has a slightly slower k_{cat} when ATP is limiting: 7.45 +/- 0.06 sec^{-1}.

The K_Ms for the family vary somewhat more widely, but newly determined values for DesD are consistent: IucA and C have K_Ms in the several hundred micromolar range[29, 30], and we found the K_M for DesD was similar (350 +/- 10 μM for dfoG). DesD's K_M for ATP is 231 +/- 4 μM, which is more than 10x tighter than the previous estimate of 3,500 μM. The specificity constant that we calculated for both dfoG and ATP evened out to nearly identical: 32,000 +/- 1,000 or 32,300 +/- 600 $M^{-1}s^{-1}$, respectively; this is well below the diffusion-controlled limit, even in glycerol, and significantly better than the 11-3,200 values reported in the family[26, 28-30], again, except for AcsD (150,000 $M^{-1}s^{-1}$)[26].

We had hypothesized that Arg306Gln would be catalytically inactive when the basic arginine was conservatively mutated to a neutral polar glutamine, based on AcsD's Arg306Lys 1.5% activity (DesD numbering), and Arg306Ala inactivity. Using our ITC assay, we confirmed this inactivity (the Arg306Gln raw data curve overlays with the heat-inactivated enzyme control nearly perfectly) and were unable to detect any activity above that baseline.

Arginine 306 was previously proposed to select for the pro-R carboxylate group in AcsD. Our model of Arginine from the wild-type structure in the active site with ATP cofactor does not contradict this analysis and would indeed be consistent—bidentate contacts at a 100° angle to the alpha phosphate position the first step of catalysis to be stereospecific, and the position of His443 and Glu467 to organize the intermediate and amine group would ensure the retention of stereospecificity in product formation. Interestingly, Glu445 had be predicted to perform the role of Glu467 from the primary structure, but is engaged with close contacts to ATP in our structure, and may be acting as a switch to trigger a small loop

to helix transition that involves His443. From the primary structure alignment, the AcsD and AsbB predicted general base position in the active site of DesD is filled with a methionine residue whose side chain is not making notable contacts to the substrate. Glu467 side chain is positioned properly to perform the AcsD observed role, but interestingly from the other side of the binding site. Future studies to explore the mechanistic role of Glu467 should also include a detailed characterization of nucleotide vs. substrate association, as this appears to be key to the turnover mechanism.

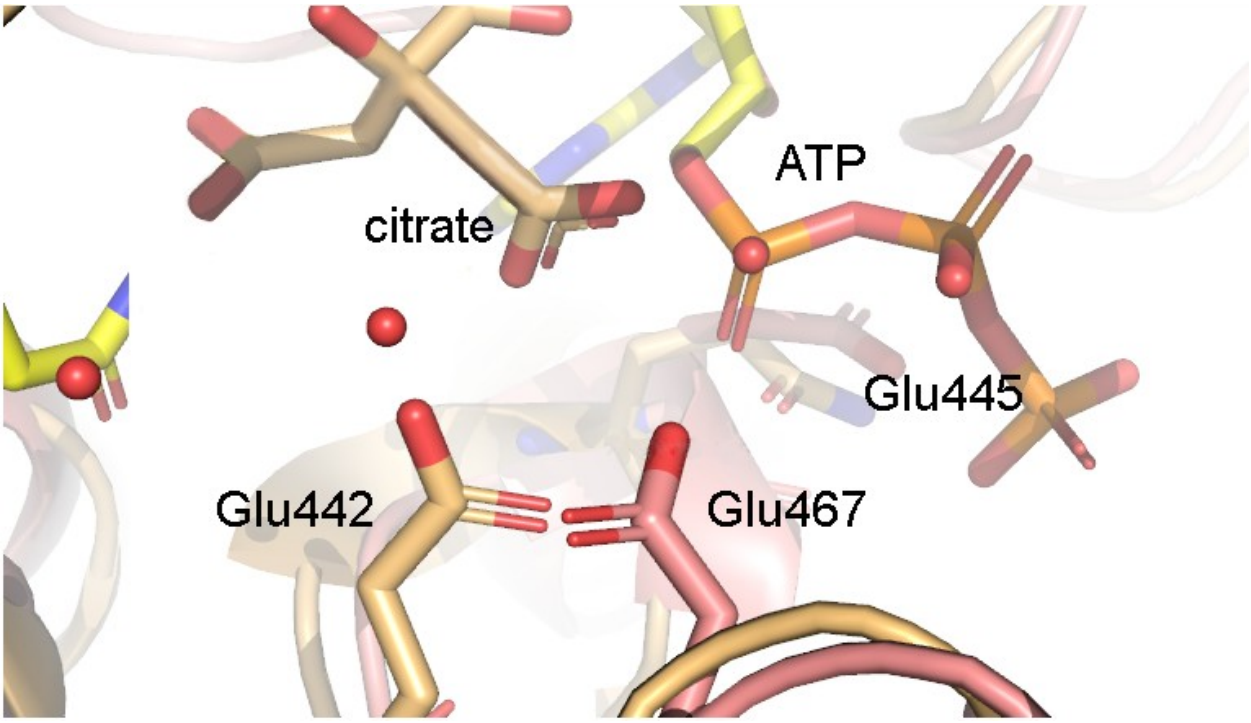

Figure 5: The role of Glu467 compared to AcsD relevant residues. DesD is shown in pink atom coloring with ATP shown in yellow atom coloring. AcsD structure 2W03 bound to citrate and ADP (not shown) is in pale orange atom coloring. AcsD catalytic residue Glu442 (AcsD numbering, shown as sticks) contacts the carboxy functional group of the substrate. The primary alignment of DesD to AcsD suggested that Glu445 (shown as sticks) would perform this role, but we observed Glu445 structurally making close binding contacts to ATP, and overlaying with the position of AscD Gln446 (shown as sticks). The residue sidechain in position to act as the catalytic glutamate is Glu467 (shown as sticks,) though the backbone position is on the opposite side of the binding pocket.

We have presented the first complete suite of cofactor structures of NIS synthetase DesD with ATP, with AMP, and in *apo* form, as well as a label-free kinetics assay that avoids the limitations of the previously utilized coupled assays and should be easily adaptable to other NIS systems. This understudied family of proteins is responsible for the synthesis of a virulence factor in the most pathogenic bacteria, and represents a prime drug target for the development of new antibiotics. Future work to delineate mechanism, subfamily variations, binding and iterative behavior should assist in developing effective inhibitors to take advantage of the bacterial need for iron.

Supporting Information:

A supplementary figure detailing the purification via GEC column and SDS-PAGE gel is available in .pdf. Additionally, an OMIT map with higher sigma levels is presented as figure S2, and a primary structure alignment with well-characterized NIS synthetase members AcsD (Type A), AsbB, IucC, AlcC and DfoC (all type C, as is DesD.)

Acknowledgements: This research was supported in part by the National Science Foundation (NSF-RUI grant 1716986 to K.M.H.), by the John Stauffer Charitable Trust for student fellowships, and by California Lutheran University. The Berkeley Center for Structural Biology is supported in part by the Howard Hughes Medical Institute. The Advanced Light Source is a Department of Energy Office of Science User Facility under Contract No. DE-AC02-05CH11231. The ALS-ENABLE beamlines are supported in part by the National Institutes of Health, National Institute of General Medical Sciences, grant P30 GM124169.

The authors would like to gratefully acknowledge the expertise and assistance of Muneera Beach at Malvern Pananalytical for ITC support and assistance, Chul Hee Kang of Washington State University,

Pullman and his students for assistance with data collection of 6P63, and Shuxing Li at the Nanobiophysics Core at University of Southern California, for ITC use.

Abbreviations: DesD, desferrioxamine synthesis protein D; dfo, desferrioxamine siderophore; ITC, isothermal titration calorimetry; NIS, Non-ribosomal peptide synthesis Independent Siderophore;

References:

[1] Neilands, J. B. (1993) Siderophores, *Arch Biochem Biophys 302*, 1-3.

[2] Braun, V., and Killmann, H. (1999) Bacterial solutions to the iron-supply problem, *Trends Biochem Sci 24*, 104-109.

[3] Neilands, J. B. (1995) Siderophores: structure and function of microbial iron transport compounds, *J Biol Chem 270*, 26723-26726.

[4] Challis, G. L. (2005) A widely distributed bacterial pathway for siderophore biosynthesis independent of nonribosomal peptide synthetases, *Chembiochem 6*, 601-611.

[5] Barona-Gomez, F., Lautru, S., Francou, F. X., Leblond, P., Pernodet, J. L., and Challis, G. L. (2006) Multiple biosynthetic and uptake systems mediate siderophore-dependent iron acquisition in Streptomyces coelicolor A3(2) and Streptomyces ambofaciens ATCC 23877, *Microbiology 152*, 3355-3366.

[6] Patel, P., Song, L., and Challis, G. L. (2010) Distinct extracytoplasmic siderophore binding proteins recognize ferrioxamines and ferricoelichelin in Streptomyces coelicolor A3(2), *Biochemistry 49*, 8033-8042.

[7] Clifton, M. C., Corrent, C., and Strong, R. K. (2009) Siderocalins: siderophore-binding proteins of the innate immune system, *Biometals 22*, 557-564.

[8] Sullivan, J. T., Jeffery, E. F., Shannon, J. D., and Ramakrishnan, G. (2006) Characterization of the siderophore of Francisella tularensis and role of fslA in siderophore production, *J Bacteriol 188*, 3785-3795.

[9] Allred, B. E., Correnti, C., Clifton, M. C., Strong, R. K., and Raymond, K. N. (2013) Siderocalin outwits the coordination chemistry of vibriobactin, a siderophore of Vibrio cholerae, *ACS Chem Biol 8*, 1882-1887.

[10] Cendrowski, S., MacArthur, W., and Hanna, P. (2004) Bacillus anthracis requires siderophore biosynthesis for growth in macrophages and mouse virulence, *Mol Microbiol 51*, 407-417.

[11] Dale, S. E., Doherty-Kirby, A., Lajoie, G., and Heinrichs, D. E. (2004) Role of siderophore biosynthesis in virulence of Staphylococcus aureus: identification and characterization of genes involved in production of a siderophore, *Infect Immun 72*, 29-37.

[12] Franza, T., Mahe, B., and Expert, D. (2005) Erwinia chrysanthemi requires a second iron transport route dependent of the siderophore achromobactin for extracellular growth and plant infection, *Mol Microbiol 55*, 261-275.

[13] Koppisch, A. T., Browder, C. C., Moe, A. L., Shelley, J. T., Kinkel, B. A., Hersman, L. E., Iyer, S., and Ruggiero, C. E. (2005) Petrobactin is the primary siderophore synthesized by Bacillus anthracis str. Sterne under conditions of iron starvation, *Biometals 18*, 577-585.

[14] Oves-Costales, D., Kadi, N., and Challis, G. L. (2009) The long-overlooked enzymology of a nonribosomal peptide synthetase-independent pathway for virulence-conferring siderophore biosynthesis, *Chem Commun (Camb)*, 6530-6541.

[15] Tripathi, A., Schofield, M. M., Chlipala, G. E., Schultz, P. J., Yim, I., Newmister, S. A., Nusca, T. D., Scaglione, J. B., Hanna, P. C., Tamayo-Castillo, G., and Sherman, D. H. (2014) Baulamycins A and B, broad-spectrum antibiotics identified as inhibitors of siderophore biosynthesis in Staphylococcus aureus and Bacillus anthracis, *J Am Chem Soc 136*, 1579-1586.

[16] Bring, P., Partovi, N., Ford, J. A., and Yoshida, E. M. (2008) Iron overload disorders: treatment options for patients refractory to or intolerant of phlebotomy, *Pharmacotherapy 28*, 331-342.

[17] Pollack, J. R., Ames, B. N., and Neilands, J. B. (1970) Iron transport in Salmonella typhimurium: mutants blocked in the biosynthesis of enterobactin, *J Bacteriol 104*, 635-639.

[18] Bergeron, R. J., and Brittenham, G. M. (1994) *The Development of iron chelators for clinical use*, CRC Press, Boca Raton.

[19] Hoette, T. M., Abergel, R. J., Xu, J., Strong, R. K., and Raymond, K. N. (2008) The role of electrostatics in siderophore recognition by the immunoprotein Siderocalin, *J Am Chem Soc 130*, 17584-17592.

[20] Kadi, N., and Challis, G. L. (2009) Chapter 17. Siderophore biosynthesis a substrate specificity assay for nonribosomal peptide synthetase-independent siderophore synthetases involving trapping of acyl-adenylate intermediates with hydroxylamine, *Methods Enzymol 458*, 431-457.

[21] Kadi, N., Oves-Costales, D., Barona-Gomez, F., and Challis, G. L. (2007) A new family of ATP-dependent oligomerization-macrocyclization biocatalysts, *Nat Chem Biol 3*, 652-656.

[22] Kadi, N., Song, L., and Challis, G. L. (2008) Bisucaberin biosynthesis: an adenylating domain of the BibC multi-enzyme catalyzes cyclodimerization of N-hydroxy-N-succinylcadaverine, *Chem Commun (Camb)*, 5119-5121.

[23] Oves-Costales, D., Kadi, N., Fogg, M. J., Song, L. J., Wilson, K. S., and Challis, G. L. (2008) Petrobactin biosynthesis: AsbB catalyzes

condensation of spermidine with N-8-citryl-spermidine and its N-1-(3,4-dihydroxybenzoyl) derivative, *Chem. Commun.*, 4034-4036.
[24] Oves-Costales, D., Song, L., and Challis, G. L. (2009) Enantioselective desymmetrisation of citric acid catalysed by the substrate-tolerant petrobactin biosynthetic enzyme AsbA, *Chem. Commun.*, 1389-1391.
[25] Schmelz, S., Botting, C. H., Song, L., Kadi, N. F., Challis, G. L., and Naismith, J. H. (2011) Structural basis for acyl acceptor specificity in the achromobactin biosynthetic enzyme AcsD, *J Mol Biol 412*, 495-504.
[26] Schmelz, S., Kadi, N., McMahon, S. A., Song, L., Oves-Costales, D., Oke, M., Liu, H., Johnson, K. A., Carter, L. G., Botting, C. H., White, M. F., Challis, G. L., and Naismith, J. H. (2009) AcsD catalyzes enantioselective citrate desymmetrization in siderophore biosynthesis, *Nat Chem Biol 5*, 174-182.
[27] Carroll, C. S., and Moore, M. M. (2018) Ironing out siderophore biosynthesis: a review of non-ribosomal peptide synthetase (NRPS)-independent siderophore synthetases, *Crit Rev Biochem Mol Biol 53*, 356-381.
[28] Nusca, T. D., Kim, Y., Maltseva, N., Lee, J. Y., Eschenfeldt, W., Stols, L., Schofield, M. M., Scaglione, J. B., Dixon, S. D., Oves-Costales, D., Challis, G. L., Hanna, P. C., Pfleger, B. F., Joachimiak, A., and Sherman, D. H. (2012) Functional and structural analysis of the siderophore synthetase AsbB through reconstitution of the petrobactin biosynthetic pathway from Bacillus anthracis, *J Biol Chem 287*, 16058-16072.
[29] Bailey, D. C., Alexander, E., Rice, M. R., Drake, E. J., Mydy, L. S., Aldrich, C. C., and Gulick, A. M. (2018) Structural and functional delineation of aerobactin biosynthesis in hypervirulent Klebsiella pneumoniae, *J Biol Chem 293*, 7841-7852.
[30] Bailey, D. C., Drake, E. J., Grant, T. D., and Gulick, A. M. (2016) Structural and Functional Characterization of Aerobactin Synthetase IucA from a Hypervirulent Pathotype of Klebsiella pneumoniae, *Biochemistry 55*, 3559-3570.
[31] Salomone-Stagni, M., Bartho, J. D., Polsinelli, I., Bellini, D., Walsh, M. A., Demitri, N., and Benini, S. (2018) A complete structural characterization of the desferrioxamine E biosynthetic pathway from the fire blight pathogen Erwinia amylovora, *J Struct Biol 202*, 236-249.
[32] Oves-Costales, D., Kadi, N., Fogg, M. J., Song, L., Wilson, K. S., and Challis, G. L. (2008) Petrobactin biosynthesis: AsbB catalyzes condensation of spermidine with N8-citryl-spermidine and its N1-(3,4-dihydroxybenzoyl) derivative, *Chem Commun (Camb)*, 4034-4036.

[33] Suarez, A. S., Stefan, A., Lemma, S., Conte, E., and Hochkoeppler, A. (2012) Continuous enzyme-coupled assay of phosphate- or pyrophosphate-releasing enzymes, *Biotechniques 53*, 99-103.
[34] Raymond, K. N., and Carrano, C. J. (1979) Coordination chemistry and microbial iron transport, *Accounts of Chemical Research 12*, 183-190.
[35] Yang, C. C., and Leong, J. (1982) Production of deferriferrioxamines B and E from a ferroverdin-producing Streptomyces species, *J Bacteriol 149*, 381-383.
[36] Berner, I., Konetschny-Rapp, S., Jung, G., and Winkelmann, G. (1988) Characterization of ferrioxamine E as the principal siderophore of Erwinia herbicola (Enterobacter agglomerans), *Biol Met 1*, 51-56.
[37] MEYER, J.-M., and ABDALLAH, M. A. (1980) The siderochromes of non-fluorescent pseudomonads: production of nocardamine by Pseudomonas stutzeri, *Microbiology 118*, 125-129.
[38] Reissbrodt, R., Rabsch, W., Chapeaurouge, A., Jung, G., and Winkelmann, G. (1990) Isolation and identification of ferrioxamine G and E in Hafnia alvei, *Biology of Metals 3*, 54-60.
[39] Smits, T. H., and Duffy, B. (2011) Genomics of iron acquisition in the plant pathogen Erwinia amylovora: insights in the biosynthetic pathway of the siderophore desferrioxamine E, *Arch Microbiol 193*, 693-699.
[40] Kontoghiorghes, G. J., Eracleous, E., Economides, C., and Kolnagou, A. (2005) Advances in iron overload therapies. prospects for effective use of deferiprone (L1), deferoxamine, the new experimental chelators ICL670, GT56-252, L1NA11 and their combinations, *Curr Med Chem 12*, 2663-2681.
[41] Loyevsky, M., John, C., Dickens, B., Hu, V., Miller, J. H., and Gordeuk, V. R. (1999) Chelation of iron within the erythrocytic Plasmodium falciparum parasite by iron chelators, *Mol Biochem Parasitol 101*, 43-59.
[42] Loyevsky, M., Lytton, S. D., Mester, B., Libman, J., Shanzer, A., and Cabantchik, Z. I. (1993) The antimalarial action of desferal involves a direct access route to erythrocytic (Plasmodium falciparum) parasites, *J Clin Invest 91*, 218-224.
[43] Buss, J. L., Greene, B. T., Turner, J., Torti, F. M., and Torti, S. V. (2004) Iron chelators in cancer chemotherapy, *Curr Top Med Chem 4*, 1623-1635.
[44] Rutschlin, S., and Bottcher, T. (2018) Dissecting the Mechanism of Oligomerization and Macrocyclization Reactions of NRPS-Independent Siderophore Synthetases, *Chemistry 24*, 16044-16051.

[45] Sarkar, G., and Sommer, S. S. (1990) The Megaprimer Method of Site-Directed Mutagenesis, *BioTechniques 8*, 404-407.
[46] Miyazaki, K., and Takenouchi, M. (2002) Creating random mutagenesis libraries using megaprimer PCR of whole plasmid, *BioTechniques 33*, 1033-1034,1036-1038.
[47] Minor, Z. O. a. W. (1997) Processing of X-ray Diffraction Data Collected in Oscillation Mode, *Methods in Enzymology 276*, 307-326.
[48] AgilentTechnologies. (2011) CrysAlisPro Software system, version 1.171.34.49 Agilent Technologies UK Ltd, Oxford, UK.
[49] McCoy, A. J., Grosse-Kunstleve, R. W., Adams, P. D., Winn, M. D., Storoni, L. C., and Read, R. J. (2007) Phaser crystallographic software, *J Appl Crystallogr 40*, 658-674.
[50] Murshudov, G. N., Vagin, A. A., and Dodson, E. J. (1997) Refinement of macromolecular structures by the maximum-likelihood method, *Acta Crystallogr D Biol Crystallogr 53*, 240-255.
[51] Emsley, P., and Cowtan, K. (2004) Coot: model-building tools for molecular graphics, *Acta Crystallogr D Biol Crystallogr 60*, 2126-2132.
[52] Emsley, P., Lohkamp, B., Scott, W. G., and Cowtan, K. (2010) Features and development of Coot, *Acta Crystallogr D Biol Crystallogr 66*, 486-501.
[53] Winn, M. D., Isupov, M. N., and Murshudov, G. N. (2001) Use of TLS parameters to model anisotropic displacements in macromolecular refinement, *Acta Crystallogr D Biol Crystallogr 57*, 122-133.
[54] Joosten, R. P., Long, F., Murshudov, G. N., and Perrakis, A. (2014) The PDB_REDO server for macromolecular structure model optimization, *IUCrJ 1*, 213-220.
[55] E.Krissinel. (2012) Enhanced Fold Recognition using Efficient Short Fragment Clustering,, *J. Mol. Biochem. 1*, 76-85.
[56] Berman, H. M., Westbrook, J., Feng, Z., Gilliland, G., Bhat, T. N., Weissig, H., Shindyalov, I. N., and Bourne, P. E. (2000) The Protein Data Bank, *Nucleic Acids Res 28*, 235-242.
[57] Engh, R. A., and Huber, R. (1991) Accurate bond and angle parameters for X-ray protein structure refinement, *Acta Crystallographica Section A 47*, 392-400.

For Table of Contents use only: